CURRENT ADVANCEMENTS OF NUMERICAL METHODS AND EXPERIMENTAL MEANS FOR THE INTEGRATION OF FUTURE PROPULSION SYSTEMS.

F. Boden[1], T. Ahlefeldt[1], R. Geisler[1], R. Meier zu Ummeln[2], A. Moreau[2], M. Norambuena[3], A. Schröder[1], C. Spehr[1], A. Stürmer[4]

DLR – German Aerospace Center

(1) Institute of Aerodynamics and Flow Technology, Göttingen, fritz.boden@dlr.de
(2) Institute of Propulsion Technology, Berlin
(3) Institute of Aeroelasticity, Göttingen
(4) Institute of Aerodynamics and Flow Technology, Braunschweig

Abstract: To integrate advanced propulsion systems and to assess and verify the related benefit (e.g. fuel burn, noise) suitable design, evaluation and measurement tools are required. For that reason, the so-called Cross-Capability-Demonstrator (XDC) has been set up as one major activity of the Large Passenger Aircraft (LPA) Platform 1 of the Clean Sky 2 initiative. The XDC is intended to demonstrate high-fidelity CFD-tools, further developed prediction tools for noise and aero-elastics as well as advanced testing tools for measuring e.g. the flow field, the deformation and the acoustics. The article will provide an update on activities within the XDC and presents some examples of recent accomplishments related to this demonstrator.

1. INTRODUCTION

Whenever existing designs are further developed or new approaches are introduced it is important to know about their impacts and benefits. As far as this principle is also valid for the integration of advanced propulsion systems or key technologies for hybrid laminar flow, both being in the focus of the Clean Sky 2 Large Passenger Aircraft program (CS2 LPA) an additional Cross-Capability-Demonstrator (XDC) stream was introduced. Within the XDC thus numerical and experimental means are further developed and demonstrated in order to use them for the assessment and verification of the benefits of future advanced propulsion systems with respect e.g. to fuel burn or noise.

The importance of this work becomes more and more relevant if limited information is available about engine products or novel flow control methods but the external assessment of technologies is still required. This for instance is the case when a research institute or engine manufacturer intends to evaluate the potential of engine noise reduction methods, or when an aircraft manufacturer needs to understand the behavior of the engines powering their airplanes. E.g. for engine fan noise the evaluation at the preliminary level is either realized with empirical correlations, such as those gained at NASA during the 1970's [1] and 1990's [2], or with more physics- and less data-based approaches such as the DLR in-house analytical tool PropNoise [3]. In both methods, the aerodynamic quantities mandatory for the fan acoustic calculation (e.g. flow velocity, blade wake size, flow turning) cannot be provided by a CFD simulation since no detailed 3D geometry is available to describe the fan stage. Similar difficulties are present too for several other common industrial methods in numerical simulations and experimental testing for aerodynamics and aeroelastics. Since much has already been done in this area at the research institutes, the logical step now is to demonstrate advanced simulation and measurement techniques and enable the aerospace industry to apply them themselves.

The top objective of the XDC therefore is to establish design processes, assessment tools and measurement techniques applicable to different types of propulsion systems (e.g. UHBR, OR, BLI). At the end of the project the XDC therefore will provide high-fidelity CFD-tools, further developed prediction tools for noise and aeroelastics and advanced testing tools. In what follows some examples of the numerical methods and experimental means considered in the XDC are presented briefly.

2. NUMERICAL METHODS

Still in the concept and design phase of a new airframe it is important to have knowledge about the impact and benefit of the implemented novelties. Naturally no test specimen is available at this stage or it is too costly to create one. Therefore, powerful prediction and simulation tools are needed that require only preliminary information about the design, but still provide detailed insight. In the context of the XDCs "Common Numerical Method" stream such tools are being demonstrated and developed suitable e.g. for predictions on installed UHBR, numerical calculations on jet flap interference noise, boundary layer stability analyses, fan design or the prediction of aeroelastic stability. On the next pages two examples of these methods are presented briefly – the enhancement of the fan broadband noise prediction and the simulations of an installed UHBR.

2.1. Enhanced prediction of fan broadband noise with improved aerodynamic models in PropNoise

The objective of this study was to provide an improved aerodynamic model for the fan noise prediction tool PropNoise [3] which is suited for the thin and slender rotor blades that typically equip the transonic fans of medium- and long-range civil aircraft. Such blades however tend to trigger flow separation at lower speeds as soon as they are put under incidence. This typically occurs at the Approach

doi: 10.25967/570147

off-design operating condition, which is one of the three relevant points for acoustic certification. With detached flow around the rotor blades the fan stage produces more broadband noise, especially the components coming from the rotor trailing edge and the dominant wake interaction with the downstream stator vanes. The purpose of the present study is to appraise the improvements in fan broadband noise prediction that is realized with an analytical acoustic model informed by a simple aerodynamic meanline approach [3]. A specific aerodynamic model suited for the aforementioned slender rotor blades was presented and evaluated in this study.

The previous aerodynamic model used in the analytical fan-noise prediction tool, PropNoise, is of semi-empirical / semi-analytical nature [3]. It basically calculates the aerodynamic loss coefficient

$$\omega = \frac{P_{t,\mathrm{in}} - P_{t,\mathrm{out}}}{P_{t,\mathrm{in}} - P_{\mathrm{in}}}, \tag{1}$$

which is a useful quantity to determine the size of the boundary layer developing around the rotor blades and the size of the wake being convected downstream and interacting acoustically with the stator vanes. This coefficient is modelled as a sum of a viscous contribution related to the boundary layer and an inviscid contribution related to the shock system:

$$\omega = \omega_{\mathrm{visc}} + \omega_{\mathrm{shock}} \tag{2}$$

The viscous contribution is modelled as a function of a diffusion factor (linked to the flow deceleration across the blade row and to the lift coefficient). The shock contribution is modelled with a modified formula of the normal shock loss with the pre-shock Mach number being a function of the inflow Mach number and lift coefficient. In both calculations, coefficients assume empirical values not derived from theoretical considerations. This model produces relatively realistic values near the design point for the two fan test cases considered in the past (DLR UHBR fan and DLR CRISP2 CRTF fan), but its lack of theoretical background makes it perform significantly worse away from the design point and when applied to other fan test cases.

A new model is proposed, that relies more strongly on the phenomenology of the problem and that includes some physically sound theoretical considerations. Rather than separating between viscous and shock losses, the new model distinguishes between the loss generated in the forward part of the blades (approximately from far upstream to the throat station at the entry of the blade passage) and the loss generated inside the blade passage up to the trailing edge of the blades:

$$\omega = \omega_{\mathrm{LE}} + \omega_{\mathrm{TE}} \tag{3}$$

As the exit flow in a compressor blade row is typically fully subsonic, the rearward-part loss $\omega_{\mathrm{TE}} = \omega_{\mathrm{TE}}{}^{\mathrm{visc}}$ is fully viscous, which means related to the boundary layer, so there is no shock loss in this region. This term primarily scales with the skin friction and with the wetted surface of the blades; it is weakly dependent of operating conditions (incidence and Mach number).

The forward-part loss ω_{LE} is calculated based on a model proposed independently by Freeman & Cumpsty (1992) [4] and Kramer & Stanitz (1955) [5].

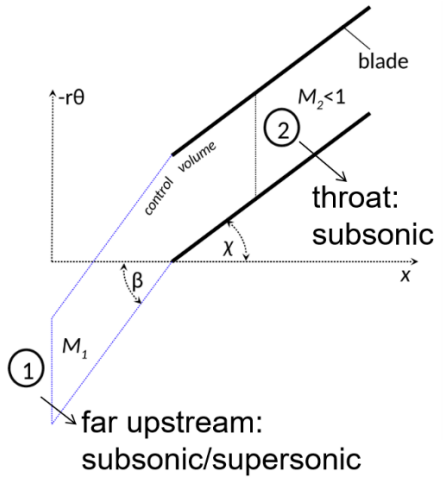

Figure 1: Modelling of fan rotor blades as flat plates and control volume analysis.

It assumes flat plates with zero thickness and with a stagger angle, as represented in Figure 1. A control volume analysis is carried out in the region between far upstream and the region near the entry of the blade row. In this volume conservation of mass, enthalpy, and momentum in blade direction is applied. As the skin friction on the blade surface is neglected in this region, and the leading edge has no thickness, the force along the blade direction vanishes which greatly simplifies the derivation of an analytical solution. From these assumptions, it is therefore possible to determine analytically the subsonic Mach number inside the blade passage M_2 and the loss produced in that region ω_{LE}. In contrary to ω_{TE}, this term is very sensitive to the inflow Mach number M_1 and blade incidence angle. At this point, as the derivation is the result of a control volume analysis, there is no clue about the nature of the loss (viscous or shock-related). A separation is however required to evaluate the overall boundary layer thickness. It is assumed that the viscous contribution is the loss that would be generated in incompressible $\omega_{\mathrm{TE}}{}^{\mathrm{visc}} = \omega_{\mathrm{TE}}{}^{\mathrm{incomp}}$, the difference being the shock loss $\omega_{\mathrm{TE}}{}^{\mathrm{shock}} = \omega_{\mathrm{TE}} - \omega_{\mathrm{TE}}{}^{\mathrm{incomp}}$.

Finally, the total viscous loss coefficient is calculated as the sum of the forward-part and rearward-part contributions:

$$\omega_{\mathrm{visc}} = \omega_{\mathrm{LE}}{}^{\mathrm{visc}} + \omega_{\mathrm{TE}}{}^{\mathrm{visc}}. \tag{4}$$

The following Figure 2 presents a comparison of the variations in loss coefficient and its respective viscous and shock components as they are predicted by the previous empirical model and by the new more physically sound model. At subsonic Mach number (here M=0.6), the new model predicts a stronger sensitivity of the overall loss coefficient to incidence than the original model, especially in the direction of positive incidence (toward fan stall), which is more relevant for the acoustic certification operating points. The strong sensitivity to the incidence is attributable to the sharp leading edge, that generates a flow separation at low speeds, whereas blades with a rounded leading edge can sustain higher incidence angles without flow separation. At supersonic Mach number (here M=1.1), the sensitivity of the overall loss coefficient is even stronger than at low speed, but here the shock system is responsible for most of the loss and only a small fraction is attributed to the viscous component, which is only weakly dependent on incidence.

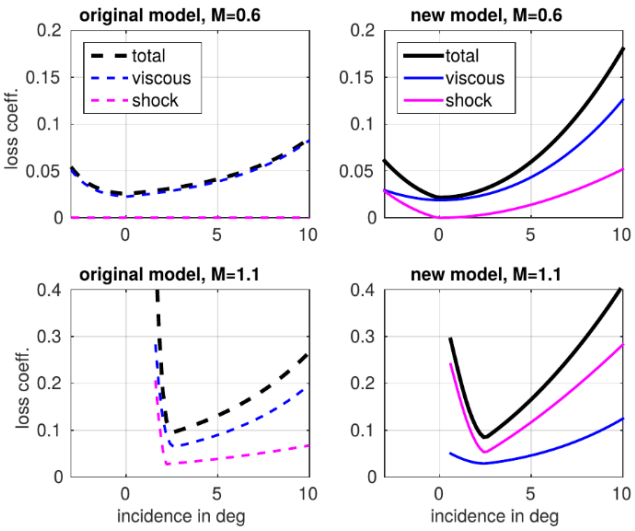

Figure 2:Comparison of the original and new aerodynamic loss models – loss characteristics of an example fan rotor for one subsonic and one supersonic inflow Mach number.

The original model, however, predicts a larger rise of viscous loss with incidence and an unrealistic weak dependence of shock loss to that parameter.

In a study it was shown that the stronger sensitivity of viscous loss to incidence at low speed, and at the same time the relatively weak dependence of viscous loss to incidence at high speed, are two physical characteristics observed on a realistic transonic fan CFD simulation, and that those characteristics are better reproduced by the new aerodynamic flat-plate model than with the original highly empirical model. The implications in terms of fan broadband noise prediction was also detailed in this study.

An overview of the assumptions underlying the new model is given here. The flat-plate aerodynamic loss model is suited for:

- Thin and weakly cambered blades with a sharp leading edge (flat plate assumption)
- Blade row with 'high enough' solidity: a flow passage between two adjacent blades should be identifiable (1D flow assumption)
- Typically fan rotor blades of highly subsonic or transonic fans fulfil these assumptions in the outer part of the blades (>60% of span)

For stator vanes however, the profiles are designed to operate at subsonic speed with a large tolerance to non-zero incidence, therefore are highly cambered and have a rounded nose. In that case, applying the new model would overestimate the sensitivity to incidence of stator wakes (and stator trailing edge and its interaction with downstream blade rows)

2.2. Simulation of installed UHBR

In the context of an increased focus on fuel efficiency and environmental impact, turbofan engine development trends continue towards larger bypass ratio engine designs, with Ultra-High Bypass Ratio (UHBR) engines becoming a likely power plant option for future commercial transport aircraft.

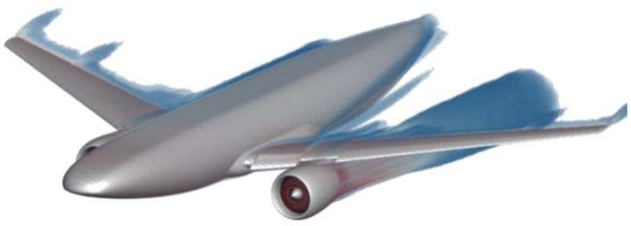

Figure 3: ONERA NOVA aircraft in high-lift configuration with the underwing-installed ASPIRE UHBR.

These engines promise low specific fuel consumption at the engine level, but the resulting size of the nacelle poses challenges in terms of the installation on the airframe. Thus, their integration on an aircraft requires careful consideration of complex engine airframe interactions impacting performance, aeroelastics and aeroacoustics on both the airframe and the engine sides. Building on work performed in the frame of the Clean Sky 2 project ASPIRE [6] [7] [8] where an isolated reference UHBR engine was studied in depth at various key operating conditions, work presently under way in Clean Sky 2 is addressing the critical aspects of installation effects on both the UHBR engine as well as the aircraft performance. The aircraft chosen for use by the Clean Sky 2 partners collaborating in this work is based on the ONERA NOVA configuration [9] For the work performed at the DLR Institute of Aerodynamics and Flow Technology, the aircraft features an ONERA-designed high-lift system consisting of leading edge slats and trailing edge flaps in settings appropriate for the climb phase of the flight mission. The ASPIRE-based UHBR engine is mounted in an under-wing type installation, as shown in Figure 3.

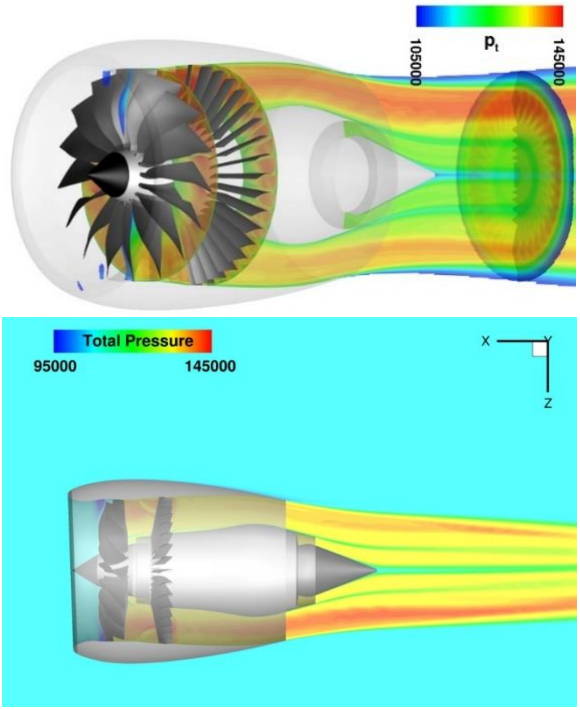

Figure 4: Isolated ASPIRE engine non-axis symmetric flow and jet development due to non-uniform fan inflow conditions for high angle of attack at sideline operating conditions.

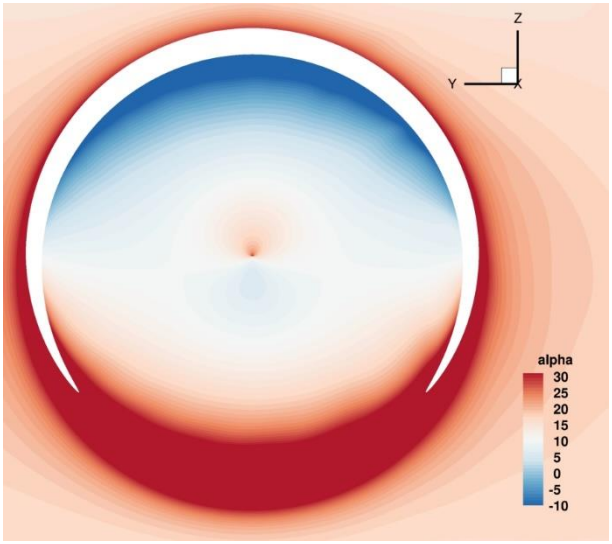

Figure 5: Isolated ASPIRE engine intake angle of attack distribution at the Sideline operating point.

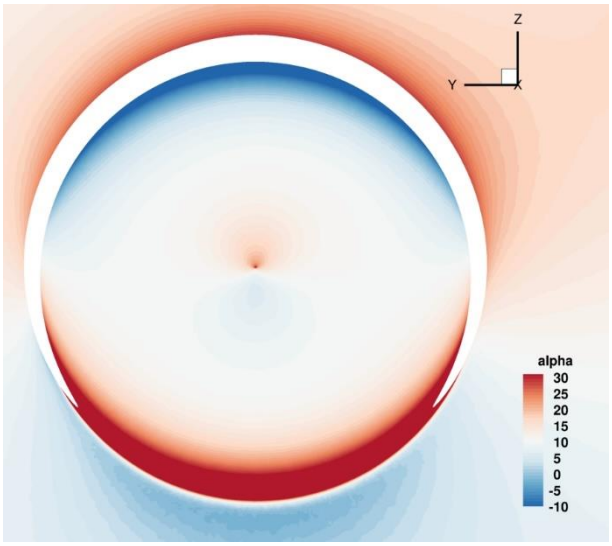

Figure 6: Engine intake angle of attack distribution for the complete aircraft at the sideline operating point and an aircraft incidence angle of 7°.

Due to the need to keep viscous drag forces acting on the nacelle low, UHBR engines will require the use of compact nacelle designs. Invariably this will also lead to shorter inlet lengths than typical of current high-bypass turbofan engines. This will reduce the inlets capability to ensure a uniform flow field is present at the axial location of the fan. As evident in Figure 4, which shows results from the ASPIRE project of the isolated UHBR engine at sideline operating conditions, the high angle of attack for the engine alone already subjects the fan to notable flow non-uniformity. Already an important aspect from the perspective of fan performance, the resulting non-axis symmetric bypass stream flow and jet may also be an important consideration for the interaction of the engine flow field with the aircraft, in particular the trailing edge high-lift system. In preparation for a high-fidelity CFD analysis featuring a fully geometrically modeled rotating fan representation in a uRANS simulation for the complete aircraft configuration using the DLR TAU-Code, very similar to those performed in the ASPIRE project, RANS studies have just been completed.

These utilized classical engine boundary conditions for the fan intake as well as the bypass and core flow exhausts and were aimed at analyzing and understanding the aircrafts high lift aerodynamics on the one hand and determining an appropriate angle of attack for the planned studies on the other, to ensure a good comparability with the existing isolated engine results available from the ASPIRE project. Due to the more complex intake flow field for the engine installed on the aircraft, driven in large part by the upwash of the wing flow, matching the exact inflow conditions as found for the isolated engine was the first task addressed in the present work.

Drawing from the flow field solutions of the complete aircraft RANS simulations at several angles of attack, the best possible agreement between the engine intake flow fields for the fully installed case (shown for the example of an angle of attack of 7° in Figure 6) with those that were seen for the isolated engine in the uRANS simulations performed in the frame of the ASPIRE project at the same sideline engine operating condition (shown in Figure 5) was identified.

The uRANS simulations for the full aircraft, which will commence shortly, will then allow for an in-depth understanding of installation effects on both the UHBR engine as well as the aircraft aerodynamic performance. With project partners performing comparable studies for additional flight and engine operating points, the resulting broad scope of data, with comparison to the isolated engine results from the ASPIRE project, will enable an in-depth aerodynamic analysis of the installation impact on UHBR engine performance and the mutual interactions with the airframe flow field.

3. EXPERIMENTAL MEANS

As soon as some preliminary geometry or generic test specimen are available modern experimental means can be used to verify the impact of the novel design, validate the numerical predictions or in an earlier stage to understand the basic physics behind the occurring phenomena. Those advanced measurement techniques tend to be less intrusive and to deliver a more detailed insight to the measured parameters. Within the XDC there is the “Common Experimental Means” stream that includes optical methods for surface pressure, shape and deformation measurements, as well as flow field investigations. Additionally, novel acoustic MEMS sensors are developed and tested and acoustic post processing tools are optimized. Last but not least also methods for vibration testing are being improved.

An example of full-scale engine flow measurements, the development of an array of acoustical MEMS microphones and the design of an active excitation system are briefly presented on the next pages.

3.1. Engine flow measurements

To demonstrate the capabilities of modern flow field measurement techniques such like stereoscopic PIV [10] for large measurement objects, a full-scale engine ground test with the DLR research aircraft ISTAR, a Dassault Falcon 2000LX, has been performed in a noise protection hangar.

Figure 7: Full scale engine flow field measurements applying stereoscopic PIV at different measurement planes (detail = inlet vortex in front of the engine).

The purpose of this test was the measurement of the flow field in selected planes at the engine inlet in several planes to generate highly accurate quantitative data for the validation of numerical methods. For the measurement setup four cameras forming two stereoscopic PIV systems have been mounted on a rigid frame close to the aircraft together with the laser optics to produce a light sheet in the measurement plane. In order to enable the measurement of several measurement planes, this frame was mounted traversable. In total 11 vertical planes sized 440 mm x 1,100 mm with a distance of 100 mm in between and 5° inclination towards the fuselage have been measured. The aircraft was standing on brakes in front of the measurement setup and the engines were powered up to 80% N1. The seeding particles, which are required for the measurement technique, have been injected several meters in front of the aircraft. Figure 7 shows an impression of the measurement with the detail of the visualization of the inlet vortex in front of the engine. In Figure 9 some of the measured flow fields in the measurement planes are depicted and Figure 8 shows a detail of the measured inlet vortex close to the fuselage. In parallel to the flow field measurements, the movement of the engine resulting from the deflection of the landing gear due to the engine thrust was measured using an additional stereoscopic camera system and markers on the nacelle. The images of these cameras have been evaluated with a similar marker detection algorithm like mentioned in [11].

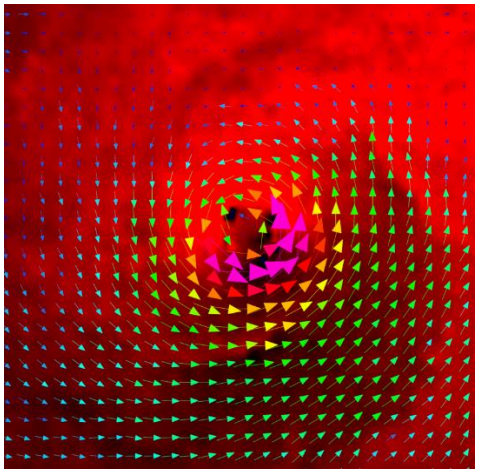

Figure 8: Example measurement result of the fuselage inlet vortex.

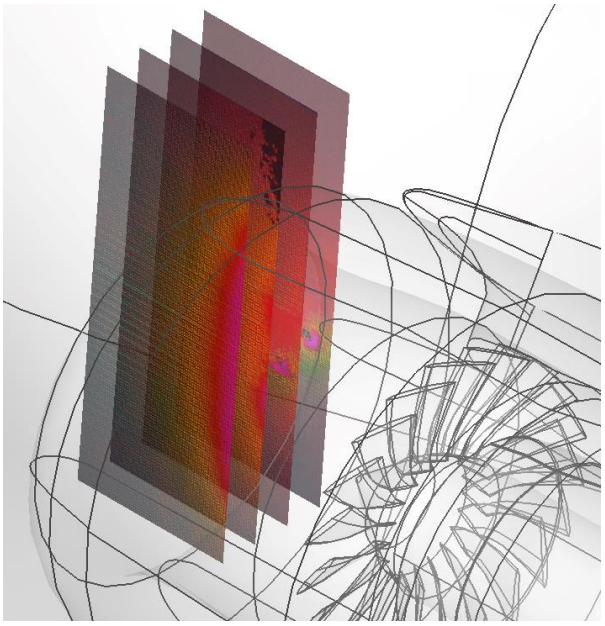

Figure 9: Determined instantaneous vector fields of four example measurement planes in front of the engine inlet.

3.2. Acoustics MEMS array

Besides the knowledge of the aerodynamic flow field and the structural behavior of an airplane also acoustics are of great interest at different operation conditions for the cabin comfort as well as for certification. Thus, aeroacoustic measurements serve two different purposes - the proof of compliance to the noise regulations but also the identification and quantification of the noise source to validate (and improve) the acoustic noise model used to predict the broadband noise. Especially out – of – flow microphone arrays are a suitable method for aeroacoustic sound source identification and have been used under various conditions [12]. Nevertheless, discrimination and separation possibility improve with the microphone array aperture and the signal to noise ration increases with the number of microphones. Furthermore, the microphones of the microphone array shall be distributed in the radiation direction of the sound sources of interest. The cost of tradition measurement microphones connected with classical data acquisition systems limits the number of available microphone channels to several hundred even for the largest systems. But recently, the DLR introduced a new microphone array system based on acoustical MEMS microphones using and FPGA as the necessary data acquisition system [13] (see Figure 10)

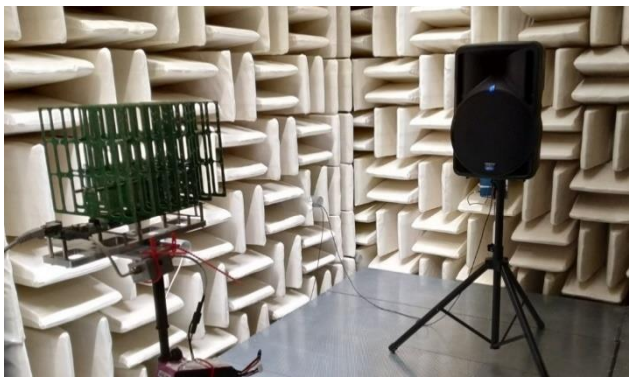

Figure 10: The PP512 MEMS array (left) tested in the anechoic room [13].

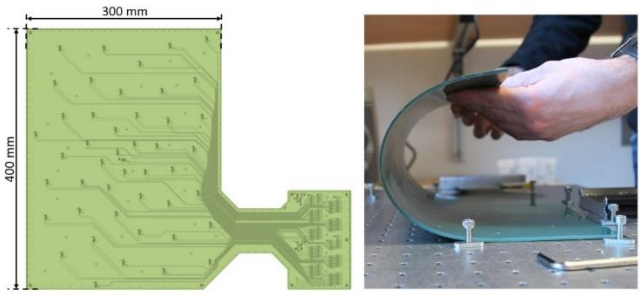

Figure 11: Overview of the flexible acoustic MEMS array (left) and demonstration of bending ability of the first prototype [15].

The system is scalable in aperture and microphone number, so a new generation of microphone array will be seen, limited only by the distribution of the microphone regarding the mean flow distribution, available space in the test section. But the real benefit might not be the improved spatial resolution or SNR due to large aperture or higher microphone number but the large distribution of microphones in space which allows to capture acoustic signals under various radiation conditions [14].

Another big advantage of the MEMS microphones is the small thickness of the sensors itself, which is below 1 mm [15]. This enables the integration of these sensors to a flexible Printed Circuit Board (PCB) which can easily been applied to aircraft structures, even with small bending radii. An example of the first prototype of such a flexible array is shown in Figure 11. This prototype was tested and improved in the laboratory and the wind tunnel and finally a first inflight application on the DLRs propeller aircraft the Dornier Do 228-101 D-CODE was performed. For the flight test the backside of the PCB was coated with silicone and a flight approved tape was used to fix it on the fuselage. Additionally, aerospace surface microphones were applied to the aircraft in order to have a reference measurement. The data acquisition system was installed in the aircraft cabin. An example the mean spectrum of the MEMS microphones and the one of the reference microphones are both shown in Figure 13. The comparison shows a good general signal agreement in the expected frequency range. The differences in the range above 2 kHz were caused by hydrodynamic pressure fluctuations. This was revealed through a wavenumber analysis.

The tests performed with the MEMS microphones and especially the flight test with the flat MEMS array demonstrated these sensors to be an inexpensive alternative to conventional microphones even under the challenging flight test conditions.

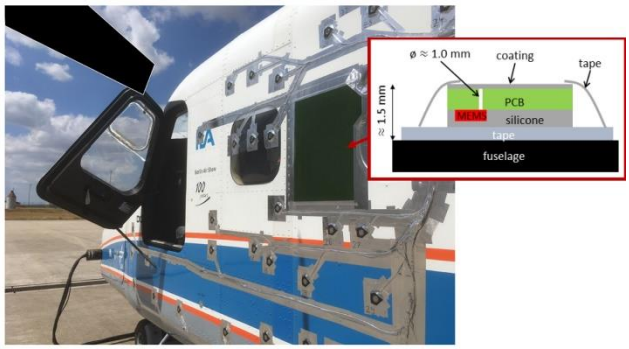

Figure 12: The MEMS microphone array mounted on the fuselage of the D-CODE and a sketch of the mounting [15].

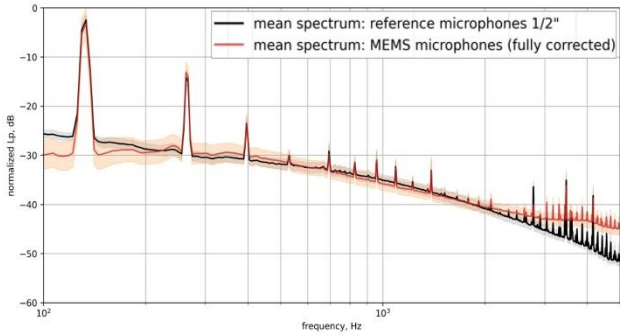

Figure 13: Comparison of the mean spectra of the MEMS microphones (red) and the reference microphones [15].

3.3. Vibration Testing

Acoustic comfort for large passenger aircrafts has become a particularly important topic in the last decades. In order to provide design decisions that help to minimize cabin noise, it is necessary to fully understand the source generation mechanisms and the transmission paths involved. The study of such problem presents a great challenge, since any experimental analysis will require numerous flight tests for data acquisition and evaluation, which means extremely high costs for research and development. If we consider that one of the most important sources of cabin noise in the low-middle frequency range are the engines, our contribution focuses on the development of an active excitation system that will mimic the vibrational behavior of those engines. Such system will help to facilitate the vibroacoustic research by allowing to replace flight tests by ground or laboratory tests.

The developed system should be able to replicate the three-dimensional forces and moments, as depicted in Figure 14, introduced by a real engine into an arbitrary structure, a demonstrator structure or a real wing if necessary. The system is based on a multichannel active controller. Such system takes as input a reference model that represents the behavior of the engine and generates the control signals that are fed to the force actuators that drive the vibratory response. The moments are generated in a similar way, except for the fact that a pair of opposite forces on an attachment device is used.

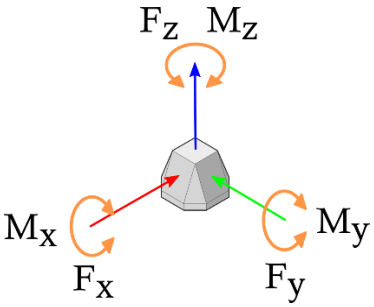

Figure 14: Schematics of forces F_X, F_Y, F_Z and moments M_X, M_Y, M_Z that the active system will control.

The control system has been developed gradually; first, a simple proof of concept was realized with a single-input single-output (SISO) force controller. Next, a multi-input multi-output (MIMO) system was able to control the injected forces in the three directions of space. Later a multi-input single-output MISO moment control system was developed. And finally, a MIMO system that combines forces and moments control. All these incremental steps

have been already described and reported in several publications [16] [17], where the latest work discusses the phase relationship of the MIMO channels.

In order to exemplify the work already performed, the latest force and moment MIMO implementation of the controller is shown. The test structure used was a single aluminum plate of 1 x 0.8 x 0.03 m, with an asymmetric milled pattern that resembles the skin fields, stringers and frames typically found in fuselage structures. The thickness of the skin fields, stringers and frames was 1, 5 and 10 mm respectively. The plate was suspended using bungee cords in order to generate free displacement boundary conditions, as seen in Figure 15.

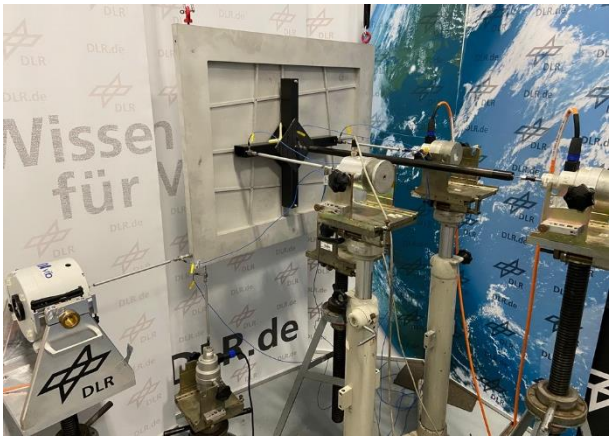

Figure 15: Aluminum plate configuration for force and moment of force control.

For the evaluation of the MIMO force and moment of force control implementation, five shakers are attached, three that apply F_x, F_y and F_z and two responsible for generating the moment in M_y direction as seen in Figure 15. In this case, four different frequency profiles were arbitrarily defined. These profiles serve as the target reference that the controller will try to replicate at the injection point of the structure. The result of the evaluation is summarized in Figure 16, where the Reference profiles and the Control ON conditions are shown. The solid and dashed lines represent the Reference and the Control ON respectively. There, it is possible to establish the correct operation of the controller. The good agreement among references and resulting profiles illustrates the proper generation of control force and moments. As seen there, it is also possible to notice an adequate signal-to-noise ratio of 15 dB that the system is able to generate. Future work will focus on the extension of the controller to a higher number of channel count in order to be able to provide all 6-Degrees of freedom that fully represent a real engine.

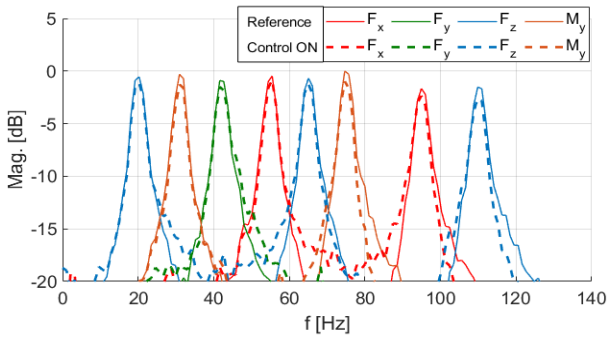

Figure 16: Spectral comparison of forces F_x, F_y, F_z and moment M_y, Reference vs. Control ON.

4. SUMMARY

In contrary to other Clean Sky 2 demonstrators of the LPA program, the Cross-Capability Demonstrator XDC is not showing only one dedicated product or method but several numerical and experimental means are developed and demonstrated for aerodynamic, aero-acoustic and structural investigations. The paper gave some examples of the current advancement of numerical methods and experimental means suitable and applicable for novel propulsion systems integration prediction, optimization and test.

In the field of numerical methods an improved aerodynamic model for the fan noise prediction tool PropNoise was presented. This flat-plate aerodynamic loss model is suited for thin and weakly cambered blades with a sharp leading edge as typical fan rotor blades of highly subsonic or transonic fans in the outer part of the span are.

With respect to the challenging numerical simulation of an installed UHBR engine an insight into the ongoing investigations was given. It reveals the significant differences in the consideration of an isolated engine with respect to an integrated one. Installation effects can be studied well that way and design rules for the future aircraft can be deduced.

Regarding the experimental means a full-scale test with an aircraft with running engines on ground was presented. A stereoscopic PIV test setup was built around the aircraft including traversable cameras and Laser, a huge seeding system in front of the aircraft and an additional position detection measurement system. The experiment enabled the researchers to measure the flow field in several planes in front of the engines inlet and investigate for instance the behavior of the fuselage inlet vortex.

In terms of the advancements of acoustic and aeroacoustic measurements the miniaturization of the sensor system using MEMS microphones was described briefly. These developments include a portable 512 MEMS microphone array for 3D intensity and beamforming measurements as well as the integration of a MEMS sensor array to a flexible printed circuit board applicable on the aircraft skin for airborne aeroacoustic measurements. Future flight test applications of the next generation flexible acoustic MEMS array are in preparation.

Last but not least the development of an active excitation system that could mimic the vibrational behavior of engines which are an important source of cabin noise. This system will help to facilitate the vibroacoustic research by allowing to replace flight tests by ground or laboratory tests.

Besides the given examples there are several other activities performed regarding non-intrusive measurements of flow, pressure or deformation and numerical tools for aeroacoustics and aeroelastics as well as boundary layer stability analyses. At the end of the project the XDC therefore will provide a couple of high-fidelity CFD-tools, further developed prediction tools for noise and aeroelastics and advanced testing tools. It is planned to summarize the results of the XDC developments in a guidance material similar to [11] in order to enable also non-experienced user to apply these means and methods for their daily work.

5. ACKNOWLEDGEMENT

This project has received funding from the Clean Sky 2 Joint Undertaking (JU) under grant agreement No 945583. The JU receives support from the European Union's Horizon 2020 research and innovation programme and the Clean Sky 2 JU members other than the Union. Furthermore the authors would like to thank all people that enable the performance of the work presented in this paper.

6. REFERENCES

[1] Heidmann, M. F. "Interim prediction method for fan and compressor source noise", NASA Lewis Research Center, Cleveland, OH, United States, Technical Report X–71763, Jun. 1979.

[2] Kontos, K. B., Janardan, B. A., Gliebe, P. R. "Improved NASA-ANOPP noise prediction computer code for advanced subsonic propulsion systems", GE Aircraft Engines, Cincinnati, OH United States, Technical Report 195480, Aug. 1996.

[3] Moreau, A. "A unified analytical approach for the acoustic conceptual design of fans of modern aero-engines", PhD thesis, Technical University of Berlin, 2017.

[4] Freeman, C., Cumpsty, N., "Method for the prediction of supersonic compressor blade performance", Journal of Propulsion, Vol. 8, pp.199-208, 1992.

[5] Kramer, J, Stanitz, J., "Prediction of losses induced by angle of attack in cascades of sharp-nosed blades for incompressible and subsonic compressible flow", NACA Technical Note 3149, 1955.

[6] Meheut, M., et al. "Assessment of Fan/Airframe aerodynamic performance using 360° uRANS computations: Code-to-Code comparison between ONERA, DLR, NLR and Airbus." AIAA Scitech 2019 Forum. 2019.

[7] Stuermer, A. "DLR TAU-Code uRANS Turbofan Modelling for Aircraft Aerodynamics Investigations". Aerospace 2019, 6, 121. https://doi.org/10.3390/aerospace6110121

[8] Schnell, R.; Goldhahn, E.; Julian, M. "Design and Performance of a Low Fan-Pressure-Ratio Propulsion System." In: Proceedings of the 25th International Symposium on Air Breathing Engines ISABE 2019, Canberra, Australia, 22–27 September 2019. Number ISABE-2019-24017

[9] Wiart, L., Atinault, O., Paluch B., Hue, D. a. G. R. "Development of NOVA Aircraft Configurations for Large Engine Integration Studies," AIAA, Paper No. 2015-2254, 2015.

[10] Raffel M., Willert C.E., Wereley S.T., Kompenhans, J. " Particle Image Velocimetry: A Practical Guide", 2nd edn. Springer, Berlin, 2007

[11] Kucaba-Pietal, A., Stasicki, B., Politz, C., Roloff, C., Boden, F., Jentink, H., de Groot, K., Szumski, M., Valla, M., Póltora, P., Szczerba, P., James, S., Kirmse, T., Weikert, T. "AIM 2 Advanced - Flight Testing Workshop. HANDBOOK of ADVANCED IN-FLIGHT MEASUREMENT TECHNIQUES". BoD – Books on Demand, Norderstedt 2013. ISBN 978-3-7322-3740-1.

[12] Merino-Martínez, R., Sijtsma, P., Snellen, M., Ahlefeldt, T., Antoni, J., Bahr, C. J., Blacodon, D., Ernst, D., Finez, A., Funke, S., Geyer, T.F., Haxter, S., Herold, G., Huang, X., Humphreys, W.M., Leclère, Q., Malgoezar, A., Michel, U., Padois, T., Pereira, A., Picard, C., Sarradj, E., Siller, H., Simons, D.G., Spehr, C. "A review of acoustic imaging methods using phased microphone arrays", CEAS Aeronaut J 10, 197–230 (2019). https://doi.org/10.1007/s13272-019-00383-4

[13] Ernst, D., Geisler, R., Kleindienst, T., Ahlefeldt, T., Spehr, C. "Portable 512 MEMS-Microphone-Array for 3D-Intensity-and Beamforming-Measurements using a FPGA based Data-Acquisition-System", 8th Berlin Beamforming Conference 2020, 02. - 03.03.2020, Berlin, Germany.

[14] Ahlefeldt, T., Spehr, C., Berkefeld, T., Di Marco, A., Burghignoli, L. "A tomographic directivity approach to frequency domain beamforming" In: AIAA Aeroacoustic Conference 2018 (2808), pages 1-13. AIAA. AIAA Aeroacoustic Conference, 25th – 29th of June 2018, Atlanta, USA. doi: 10.2514/6.2018-2808.

[15] Ahlefeldt, T., Haxter, S., Spehr, C., Ernst, D., Kleindienst, T. „Road to Acquisition: Preparing a MEMS Microphone Array for Measurement of Fuselage Surface Pressure Fluctuations". Micromachines 2021, 12, 961. https://doi.org/10.3390/mi12080961

[16] Norambuena, M., Winter, R., Biedermann, J. "Accurate structural excitation through adaptive control," in International Conference on Noise and Vibration Engineering ISMA 2018, Leuven, 2018.

[17] Norambuena, M., Winter, R., Biedermann, J. "Inverse control applied to structural excitation systems," in DAGA 2018 - 44. Jahrestagung für Akustik, München, 2018.

[18] Norambuena, M., Winter, R. "An adaptive structural excitation system as a tool for structure-borne noise research," in ICA 2019 - 23rd International Congress on Acoustics, Aachen, 2019.

[19] Norambuena, M., Winter, R. "Active structural excitation as known source for structure-borne noise research.," in INTER-NOISE 2019, Madrid, 2019.

[20] Boden, F., Barth, H. P., Hein, S., Heitmann, D., Kirmse, T., Klein, C., Krüger, W., Lemarechal, J., Norambuena, M., Schäfer, D., Schnell, R., Sinha, K., Theiß, A., Weiss, A. "Recent developments of common numerical methods and common experimental means within the framework of the large passenger aircraft programme," in Deutscher Luft- und Raumfahrtkongress (DLRK), Bremen, 2021.

[21] Norambuena, M., Winter, R., Böswald, M. „Smart Structural Excitation: Simplifying Vibroacoustic Research " Deutscher Luft- und Raumfahrtkongress (DLRK), Dresden, 2022.